OPEN ACCESS Freely available online

IJCMB
International Journal of Clinical Medicine and Bioengineering

ISSN 2737-534X
Volume 2, Issue 2
https://www.iikii.com.sg/journal/IJCMB
International Journal of Clinical Medicine and Bioengineering

Article

Changes in Functional Activity of Rabbit's Retina During Flicker Photostimulation with Scale-free Dynamics

Vladimir V. Neroev [1], Marina V. Zueva [2,*], Natalia V. Neroeva [1], Denis V. Fadeev [3], Irina V. Tsapenko [2], Tatiana D. Okhotsimskaya [1] and Vladislav I. Kotelin [2]

[1] Department of Retinal and Optic Nerve Pathology, Helmholtz National Medical Research Center of Eye Diseases, Str. Sadovaya-Chernogriazskaya 14/19, 105062, Moscow, Russian Federation; secr@igb.ru
[2] Department of Clinical Physiology of Vision, Helmholtz National Medical Research Center of Eye Diseases, Str. Sadovaya-Chernogriazskaya 14/19, 105062, Moscow, Russian Federation; visionlab@yandex.ru
[3] Scientific Experimental Center, Helmholtz National Medical Research Center of Eye Diseases, Str. Sadovaya-Chernogriazskaya 14/19, 105062, Moscow, Russian Federation; denis.fadeev@mail.ru
* Correspondence: visionlab@yandex.ru; Tel.: +7-916-576-23-59

Received: May 8, 2022; **Accepted:** May 28, 2022; **Published:** Jun 30, 2022

Abstract: Neuroplasticity-based stimulation therapy assists in restoring the visual system in neurodegenerative disorders. Scale-free fluctuations peculiar to healthy physiological rhythms disappear as the disease progresses. Fractal visual stimuli positively influence CNS plasticity and increase the efficiency of visual rehabilitation. To determine the effect of a lengthy course of fractal photostimulation (FS) on the electroretinogram (ERG) in healthy rabbits, a device for FS was created. For twelve healthy rabbits, 20-minute FS sessions were conducted once a day from 9 to 11 a.m., five times a week. Before and after 1, 4, and 12 weeks of FS, full-field ERGs, flicker ERGs, and the pattern-ERGs were registered. The observed positive impact of FS consisted of shortening peak latency of the maximal scotopic ERG b-wave and a significant increase in the amplitude of the cone ERG a- and b-waves and low-frequency flicker ERGs ($p < 0.05$). For the first time, we describe the effect of FS on the ERG. The long-term FS does not impair retinal activity and can be safely used in the clinic. The dynamics of the positive influence of FS on retinal activity argue that the duration of the FS course of 1 to 4 weeks is optimal for subsequent studies.

Keywords: Scale-free dynamics, Fractal photostimulation, Visual rehabilitation, Neuroplasticity, Electroretinogram

1. Introduction

Technologies for assessing and correcting visual functions and functional vision employ various types of stimulation therapy, including transcranial, transcorneal, percutaneous magnetic and electrical stimulation, stochastic electrical noise treatment, and audio and visual stimulations based on CNS plasticity [1–4]. Stimulation therapy aims to enhance adaptive plasticity and restore disturbed neural connections in the retina and brain, affecting their functions. Brain activity is susceptible to the rhythms of the external environment and adjusts itself with the synchronizing rhythm of external signals [5,6]. Thus, it is essential to consider that the physiological rhythms of a healthy organism, including the brain and individual neuron activity, have highly correlated fractal dynamics [7–11]. On the contrary, diseases and aging contribute to strictly ordered or completely random (stochastic) physiological fluctuations in rhythms [8,12–18]. Therefore, the therapeutic use of signals that are not adequate to the physiological rhythms of a healthy person must be treated with extreme caution.

Early studies showed definite effects on the retina of the temporal or geometric self-similar structures, which are related to the properties of natural fractals. Several studies expected the likelihood of their therapeutic impact. For example, studies found that artificial geometric fractals affect the dimension of EEG and the structure of fixational eye movements [19], and visual signals [20] and fractal audio and visual tones change the fractal dimension of gait in healthy individuals [20–22] and patients with Parkinson's disease [23]. The plasticity potential of nervous tissue decreases with aging and neurodegenerative diseases [24]. It weakens the effect of any neurorehabilitation technologies based on neuroplasticity mechanisms. In degenerative diseases of the retina, stimulation with scale-free optical signals of fractal dynamics is hypothesized to positively affect the plasticity of the nervous tissue, increasing the effectiveness of neuroprotection and rehabilitation [25–27]. Changes in the retina and brain manifested through the preclinical and early stages of neurodegenerative diseases are specifying adaptive plasticity while protecting the structure and

function of the nervous tissue [28,29]. Therefore, stimulatory therapy that activates adaptive plasticity assists in weakening the pathological process.

The proposed new approach to stimulating therapy corrects and restores visual functions based on complex optical signals: fractal dynamics of brightness fluctuations on the emitter screen [30]. Studying the mechanisms of the influence of fractal photostimulation (FS) on the retina and substantiating the prospects of using this approach to improve visual functions in humans requires experimental research of the FS effects in animals using various stimulation modes. Therefore, this study aims to determine the characteristic changes (if any) in the functional activity of the retina of healthy rabbits after FS with a subtask of detecting the effects and assessing the safety of fractal flicker exposure on light-evoked retinal activity. The results of the conducted study are of research-to-practice value in avoiding overdose exposure and recommending optimal FS regimens in subsequent experimental and clinical studies.

2. Materials and Methods

2.1. Animals

To minimize the participation of laboratory animals in the pilot study, the total number of rabbits was limited to 12, which was considered a sufficient amount to answer the question posed. At the same time, it allowed substantiating future studies on a larger number of samples to analyze the therapeutic effects of FS in degenerative diseases of the retina and brain. Twelve healthy rabbits of the Soviet Chinchilla breed (males) aged 2.5–3.0 months and weighing 1.7–2.1 kg for 24 eyes were supplied by the licensed nursery. The rabbits underwent three weeks of quarantine on arrival to adapt to the animal research facility (vivarium) conditions and to minimize the impact of a visual compromise prior to the pilot study. The rabbits were kept on a 12-hour light/dark cycle in individual stainless steel cages equipped with sippy cups and feeders. The cage dimensions were 35 cm tall to 47 cm wide (floor area 0.22 m^2). Conditions of animal housing and examination: air temperature of + 18–22°C and 60–75% relative air humidity.

All procedures were performed after consulting the veterinarians and under their approval of the experimental protocols. The research followed international standards requirements for using animals in non-clinic trials, including the ARVO Statement for the Use of Animals in Ophthalmic and Visual Research [31], and corresponded to Principles of Good Laboratory Practice (GLP) [32,33]. The local Ethics Committee of Helmholtz National Medical Research Center of Eye Diseases also approved the applicable research protocol. For adequate ERG recording, most laboratory animal species may require sedation or general anesthesia. In turn, that may affect the amplitude or time parameters of the visual evoked potentials in the retina and visual cortex [34–37]. Unlike other animals, rabbits easily tolerate non-invasive clinical electroretinography. However, given that rabbits are easily stressed, light sedation is recommended before the ERG procedure when the animal still resides in a familiar environment. A 2% solution of xylazine hydrochloride (Rometar, Bioveta, Inc., Czech Republic) was injected intramuscularly at the dose of 4.0 mg/kg of body weight as a pre-procedural premedication to minimize possible discomfort or distress. Limiting the rabbits' mobility during the study was necessary for obtaining a high-quality record of the retinal light-evoked potentials. Proper immobilization gave the animal a sense of security and reduces fear. Daily FS sessions without anesthesia throughout the experiments met the principles of humane treatment of animals.

2.2. Fractal Photostimulation

The FS impact on the retinal functional activity was thoroughly examined. The photostimulation was performed in periods of 1 week, 30 days, and 90 days, five times a week, excluding weekends. In experimental days, one 20-minute FS session was performed for each animal from 9 am to 12 am. Unlike in humans, the rabbit's eyes are located not in front but on the sides of the head, thus giving the animal a different viewing angle. Therefore, we created an emitter design to stimulate rabbits and other laboratory animals with fractal optical signals (Fig. 1). The position and angle of rotation of the emitters were specifically designed to easily adjust to the eyes of different laboratory animals.

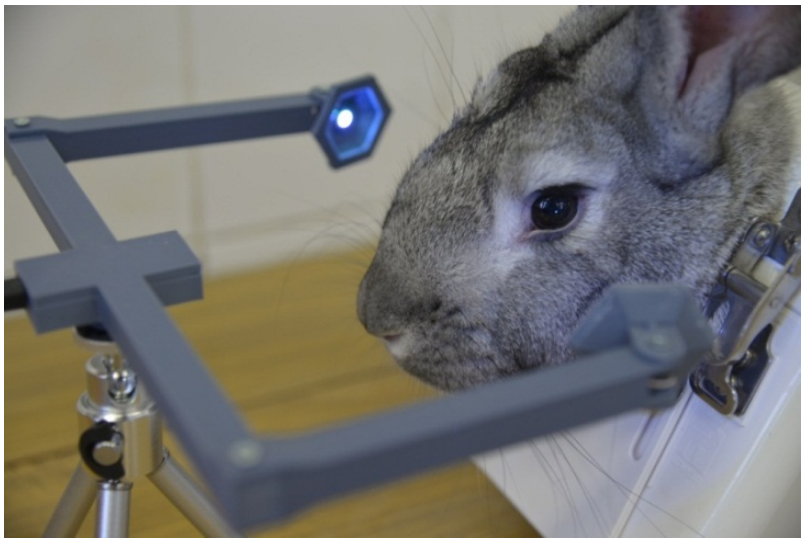

Fig. 1. Rabbit fixed in the restrainer during the fractal photostimulation.

The following representation Weierstrass-Mandelbrot function was used to calculate a fractal signal.

$$\frac{(\sigma\sqrt{2})\sqrt{1-b^{(2D-4)}}}{\sqrt{1-b^{(2D-4)(N+1)}}}\sum_{n=0}^{N}\left(b^{(D-2)n}\sin\left(2\pi\cdot s\cdot b^{n}\cdot x+2\pi\cdot rand(0,1)\right)\right) \quad (1)$$

where D - fractal dimension, σ - standard deviation, s, b - spatial-frequency scaling parameters.

The fractal signal has a self-similar structure. The signal's pattern at the next self-similarity level repeats the pattern at the previous self-similarity level with a higher frequency. Nonlinear fluctuations of signal brightness with Hausdorff-Bazikovich fractal dimension (D) in the range from 1 to 2 and a self-similarity level from 2 to 10 are created. Therefore, we used WS2812B LED – an intelligent control LED integrated light source. The datasheet for this RGB LED source includes characteristics for the red (620–625 nm), green (522–525 nm), and blue (465–467 nm) components [38]. The signal power during fractal stimulation fluctuated from 0 to 40 units on a scale from 0 to 255 (the maximum). The measured actual maximum illuminance after passing through the device and before entering the eyes (for rabbits at a distance of 10–15 cm from the emitters) was 8–12 lx (varied 0:8–12 lx). The FS device produced a light close to white. However, the RGB colors in the WS2812B were mixed at the same emitting power for each color. Therefore, the final wavelength of the radiation could not be strictly white for the observer.

As the signal conditioning instrument, an Arduino controller was used. The controller had technical limitations. In particular, we could not switch the signal with an infinite frequency, which limited the adjustment of the ratio of the frequency of the first pattern, the level-to-level frequency multiplication factor, and the number of self-similarity levels. The technical device that we made allowed switching brightness levels no more often than once every 50 ms or with 20 kHz. It generated a discrete signal where the minimum switching time between signal levels was 50 ms. The literature data substantiated the FS parameters as optimal parameters for their subsequent translation to the clinic. The frequency of the signal pattern of 9–11 Hz was chosen at the first self-similarity level. In the study, a fractal signal was used in which the pattern frequency increases of each next self-similarity level by 2.5 times (b = 2.5).

It has been shown in several works that flickering visual stimuli changed cortical activity and improved episodic memory. In particular, flickering with a 9.5–11.0 Hz frequency facilitated memorization and recalling of monosyllabic words in young and elderly adults [39,40]. In the elderly, cognitively healthy people, recalling words for a long time after their memorization was significantly improved only after the presentation of flashes with a frequency close to 10.2 Hz, but not lower than 9.0 or higher than 11.0 Hz [39].

For clinical trials, we examined the effects of FS in healthy animals using a known safe intensity and mean fractal dimension corresponding to the FD of fractals with a maximum aesthetic appeal (Taylor *et al.*, 2005, and discussion in Section 4.3). We chose for the experiment only one value D = 1.4 as it may be optimal to ensure the maximum therapeutic effect in future clinical studies, considering the literature data and the results of our studies. Previously, we showed a clinically significant impact of a two-week

course of fractal phototherapy (with the same D value and LED stimulus parameters) in patients with glaucoma in the course of limited clinical trials approved by the Local Ethics Committee of the Voronezh State Medical University [41].

We used the low intensity of light radiation since we studied a future therapeutic method for which even potentially damaging exposure levels were unacceptable. By offering new therapeutic options, we must not violate established safety standards.

2.3. Optical Coherent Tomography of the Retina

Optical coherent retinal tomography was performed with the Spectralis HRA+OCT device (Heidelberg Engineering, Germany) (Chen *et al.*, 2005). The survey was conducted under the Line and Macular Map protocols. This technique allows for obtaining high-quality images of the rabbit retina with credible verification of the retinal layers. The rabbits were fixed so that the visual streak, located approximately 3 mm ventral to the optic nerve head, appeared in the center of the image [42–44]. SD-OCT studies were carried out, too, in dynamics before and after the courses of fractal phototherapy: 1 week, 1 month, and 3 months. Quantitative analysis was performed by using the Macular Map protocol. Using this protocol in humans allows for analyzing the entire thickness of the retina and layer-by-layer segmentation in an automatic mode. The most correct and reproducible results were obtained for the entire thickness of the neuroepithelium. For rabbits, layer-by-layer analysis of the retina was also possible, but qualitative analysis of the scans showed that the quantitative results were not entirely correct as segmentation was carried out automatically.

2.4. Electroretinography

Electroretinographic studies were performed via RETIport/scan21 diagnostic system (Roland Consult, Germany) in the light-proof recording cabin shielded against electromagnetic interference. The rabbits were swaddled with a warm towel to maintain body temperature. The restrainer for laboratory animals was used to fix rabbits during electroretinography. The retainer was located on a platform at the Ganzfeld dome so that the rabbit head fit inside the stimulator dome. The scotopic and photopic full-field ERGs were recorded simultaneously from both eyes during binocular stimulation. The procedure included animals preliminarily dark-adaptation for 30 min. Then, under dim red light illumination, we dilated the pupils with the combination of 0.8% tropicamide and 5% phenylephrine hydrochloride (Appamide) solutions. 0.5% proxymetacaine solution was applied to anesthetize the cornea and 1.4% hydroxyethyl cellulose (conductive medium) to prevent corneal drying. Next, an ERG-Jet contact lens (Fabrinal, Switzerland) was placed on the cornea as the active electrode. Stainless steel needle electrodes (0.4 × 13 mm) served as the reference and ground electrodes, being placed in the forehead area between the two eyes subcutaneously, ipsilateral to the recording electrode. The recording was conducted at the impedance value below 2 kΩ. Both the research methodology and conditions for registering potentials comply with the ISCEV (International Society for Clinical Electrophysiology of Vision) standards for human research [45] and have proper regard for the features of ERG testing in rabbits [46].

The pattern-ERGs (PERGs) were recorded with the rabbit's monocular stimulation, and the right eye was examined first. Transient PERGs and steady-state PERGs [47] were recorded as a response to the reversing black-and-white chess patterns with a contrast of 97% and the rate of reverse 2 and 8 rev/s, angular sizes 16°, 0.8°, and 0.3°. The scotopic and photopic full-field ERGs were recorded simultaneously from both eyes during binocular stimulation. The animals were preliminarily dark-adapted for 30 min. First, the ERGs were recorded under the conditions of dark adaptation for the stimulus strength of 0.01 photopic $cd \cdot s \cdot m^{-2}$ (dark-adapted 0.01 ERG, rod-system response) and a standard stimulus 3.0 photopic $cd \cdot s \cdot m^{-2}$ (dark-adapted 3.0 ERG or the mixed rod-cone ERG). Then, the rabbits adapted for more than 10 min to the illumination of 30 photopic $cd \cdot m^{-2}$, and a photopic (cone) ERG was recorded against this light background to a standard stimulus at the frequency of 1 Hz. Afterward, in the same photopic conditions (light adaptation, light background, and standard stimuli), photopic flicker ERGs were registered while evoked by flashes with the frequency of 8.3, 10, 12, and 24 Hz, delivered on the light background of 30 $cd \cdot m^{-2}$ [48]. The first set of ERG recordings was obtained several days before the course of FS. Further determination of whether the retinal functional activity changes with photostimulation courses of varying duration required three more sets of FS, recorded at days 7, 30, and 90 for follow-up. Testing was performed at the same time of the day, from 9:00 am to 12:00 am, to avoid circadian influences on the retinal light-evoked responses.

2.5. Data Analysis

The experiment design involved pilot studies performed on the minimum number of animals necessary to obtain data without compromising scientific quality. Phototherapy sessions were performed for both eyes. The initial data of the studied ERG parameters before the phototherapy courses were taken as the control values. Each ERG recording was repeated two to five times until reaching two identical curves to ensure reproducibility followed by the analysis of the amplitude and culmination time (peak latency) of the scotopic and photopic ERGs waves. In the mixed rod-cone ERG and the cone ERG, the amplitude of the a-wave was

measured from the baseline to the negative minimum and the amplitude of the b-wave measurement from the a-wave peak to the positive peak of the response (positive maximum). The rod ERG b-wave was measured from baseline to the b-peak because no a-wave was identified in the rod response to weak flash. The peak latencies of the ERG waves were measured from the onset of the stimulus to their peaks. The 'b/a' index was calculated as the ratio of the amplitudes of the ERG a- and b-waves.

The choice of sample size in the pilot study was determined by the need to use the minimum number of animals recruited into the experiment but at the same time be sufficient to solve the problem [31]. For the same reason, to limit the necessary number of samples, we did not include the contralateral eye as a control using the data from both eyes for statistical analysis (24 eyes of 12 rabbits). Under the proposed specific experimental design, both eyes underwent photostimulation. Thus, the original research data obtained before photostimulation served as an appropriate control.

Statistical analysis was performed by using Microsoft Office Excel 2016 (Microsoft, USA) and Statistica 10.0 software (TIBCO Software Inc., Version 13.3). For quantitative variables, a normality test was performed. When the distribution of the studied values was close to normal, the Student's t-test determined the effect of fractal phototherapy on retinal function. The significance of the differences at critical threshold values of $p < 0.05$ was assessed. Besides, the significance of differences (p) for unrelated samples was determined by nonparametric methods (The Mann-Whitney U test). Thereby, in the tables, the data are presented as the M ± 1SD (mean ± standard deviation), medians, and percentiles (Q25 and Q75).

3. Results

3.1. Optical Coherence Tomography of the Retina

The data showed no dynamics of OCT parameters revealed in the rabbit retina during the follow-up period. The retina thickness remained stable. Before the treatment, the total thickness of the rabbit retina in the group averaged 168.2 ± 1.0 μm. Subsequently, it practically did not change and amounted to 168.8 ± 2.6, 166.5 ± 3.7, and 168.5 ± 3.1 microns (M ± SD) after 7, 30, and 90 days of observation, respectively. The noticed minor fluctuations in retina thickness were not statistically significant and did not go beyond the permissible measurement error of the device. A qualitative analysis of the tomograms showed no pathological changes in the retinal layers during the full observation period. The layers of the neuroepithelium were visualized clearly along the entire length. The differentiation of the layers was not impaired.

3.2. Electroretinography

Tables 1–5 include the results of parametric and nonparametric statistical analysis of the dataset obtained before (0) and after fractal photostimulation courses of one- (1w), four- (4w), and twelve-weeks (12w) courses. Nonparametric statistical analysis confirmed general patterns similar to those established when analyzing the mean values and standard deviations. The results of the study showed the absence of statistically significant deteriorations in the amplitude and time parameters of all recorded types of ERG but some positive effects of FS on retinal activity were noted. No significant changes were found in the peak latency of the P50 and N95 waves of the transient PERG in any FS duration (not shown in the tables). The amplitudes of the transient PERG P50 and N95 (Table 1, Fig. 2), and the steady-state PERG (Table 2) increased slightly after one month of the FS course. Still, these changes were insignificant or low significant. The largest increase in amplitude was found for the PERG N95 component for the 16 ° stimulus.

Table 1. Transient pattern ERG.

16°, P50 amplitude, μV									
Data Set	**Mean**	**Student's t-test**	**SD**	**Min**	**Max**	**Q25**	**Median**	**Q75**	**Mann-Whitney U-test**
0	13.98333		2.946467	11.20000	19.00000	11.80000	13.25000	15.40000	
1w	12.76667	$p = 0.432889$	5.326788	6.30000	18.40000	7.50000	13.40000	16.00000	0.818182
4w	17.01667	$p = 0.197079$	3.217090	12.30000	20.50000	14.80000	17.00000	20.50000	***0.093074***
12w	14.05000	$p = 0.979283$	3.646459	9.40000	18.30000	11.70000	14.25000	16.40000	0.99999
16°, N95 amplitude, μV									

Table 1. *Cont.*

Data Set	Mean	Student's t-test	SD	Min	Max	Q25	Median	Q75	Mann-Whitney U-test
0	10.46667		6.355995	6.20000	23.10000	6.80000	8.25000	10.20000	
1w	13.56667	$p = 0.291727$	4.326045	7.70000	18.30000	10.00000	14.30000	16.80000	0.179654
4w	18.06667	**$p = 0.015850$**	4.947592	13.20000	23.20000	14.30000	17.95000	20.80000	**0.041126**
12w	12.05000	$p = 0.625754$	2.701234	9.50000	15.60000	10.20000	12.45000	13.95000	0.171429
0.8°, P50 amplitude, μV									
Data Set	**Mean**	**Student's t-test**	**SD**	**Min**	**Max**	**Q25**	**Median**	**Q75**	**Mann-Whitney U-test**
0	6,200000		1,331165	5,100000	7,600000	5,200000	5,800000	6,700000	
1w	6,033333	$p = 0.855380$	2,076215	2,800000	8,900000	4,800000	6,300000	7,100000	1.000000
4w	7,150000	$p = 0.305875$	1,221065	5,400000	8,900000	6,400000	6,950000	8,100000	0.132035
12w	8,350000	**$p = 0.046916$**	1,415392	6,300000	9,500000	7,450000	8,800000	9,250000	**0.038095**
0.8°, N95 amplitude, μV									
Data Set	**Mean**	**Student's t-test**	**SD**	**Min**	**Max**	**Q25**	**Median**	**Q75**	**Mann-Whitney U-test**
0	5.600000		3.262514	3.000000	11.80000	3.600000	4.550000	6.000000	
1w	4.300000	$p = 0.393025$	3.159114	2.100000	7.90000	2.800000	5.350000	6.300000	0.937229
4w	6.116667	$p = 0.732015$	1.421853	4.400000	7.70000	4.700000	6.200000	7.500000	0.309524
12w	7.150000	$p = 0.363027$	1.405940	5.400000	8.60000	6.050000	7.300000	8.250000	0.171429
0.3°, P50 amplitude, μV									
Data Set	**Mean**	**Student's t-test**	**SD**	**Min**	**Max**	**Q25**	**Median**	**Q75**	**Mann-Whitney U-test**
0	5.800000		3.853310	1.900000	10.10000	2.500000	5.100000	9.400000	
1w	6.300000	$p = 0.851717$	4.889581	2.100000	14.70000	3.300000	5.700000	9.500000	0.937229
4w	8.016667	$p = 0.328925$	2.395343	4.400000	11.10000	6.900000	7.900000	9.950000	0.240260
12w	4.925000	$p = 0.684170$	2.434988	1.700000	7.00000	3.050000	5.500000	6.800000	0.914286
0.3°, N95 amplitude, μV									
Data Set	**Mean**	**Student's t-test**	**SD**	**Min**	**Max**	**Q25**	**Median**	**Q75**	**Mann-Whitney U-test**
0	3.583333		3.136505	0.700000	7.600000	1.200000	2.350000	7.300000	
1w	5.033333	$p = 0.364628$	2.717106	0.800000	8.100000	3.500000	5.150000	7.500000	0.393939
4w	6.466667	***p=0.080876**	2.512900	3.700000	9.700000	4.000000	6.150000	9.100000	0.132035
12w	4.175000	$p = 0.738196$	2.126617	1.000000	5.500000	3.000000	5.100000	5.350000	0.914286

* The tendency to increase in the amplitude; Bold red – statistically significant ($p < 0.05$).

Table 2. Steady-state pattern ERG.

Steady-state pattern ERG, 16°, amplitude, μV									
Data Set	**Mean**	**Student's t-test**	**SD**	**Min**	**Max**	**Q25**	**Median**	**Q75**	**Mann-Whitney U-test**
0	11.26667		2.779688	7.100000	15.00000	10.20000	10.85000	13.60000	
1w	9.78333	$p = 0.292972$	2.491920	6.100000	12.50000	8.10000	10.05000	11.90000	0.484848
4w	13.65000	***p=0.098822**	2.037400	9.700000	15.20000	13.50000	14.30000	14.90000	0.240260
12w	12.12500	$p = 0.581930$	1.898025	9.500000	13.90000	10.80000	12.55000	13.45000	0.761905
Steady-state pattern ERG, 0.8°, amplitude, μV									
Data Set	**Mean**	**Student's t-test**	**SD**	**Min**	**Max**	**Q25**	**Median**	**Q75**	**Mann-Whitney U-test**
0	6.200000		3.228002	0.200000	9.300000	5.200000	7.300000	7.900000	
1w	7.233333	$p = 0.485083$	3.023684	1.700000	9.700000	6.200000	8.150000	9.500000	0.423340
4w	7.116667	$p = 0.535102$	1.334791	5.600000	8.900000	5.900000	7.100000	8.100000	0.818182
12w	7.750000	$p = 0.351551$	1.500000	6.500000	9.500000	6.500000	7.500000	9.000000	0.609524
Steady-state pattern ERG, 0.3°, amplitude, μV									
Data Set	**Mean**	**Student's t-test**	**SD**	**Min**	**Max**	**Q25**	**Median**	**Q75**	**Mann-Whitney U-test**
0	6.216667		3.018222	2.300000	11.20000	4.30000	6.05000	7.40000	
1w	6.116667	$p = 0.942058$	2.812413	2.100000	9.20000	3.40000	6.75000	8.50000	0.937229
4w	6.500000	$p = 0.836926$	1.353514	5.400000	8.80000	5.50000	5.95000	7.40000	0.937229
12w	6.175000	$p = 0.978389$	1.309898	4.500000	7.70000	5.35000	6.25000	7.00000	0.914286

***** The tendency to increase in the amplitude.

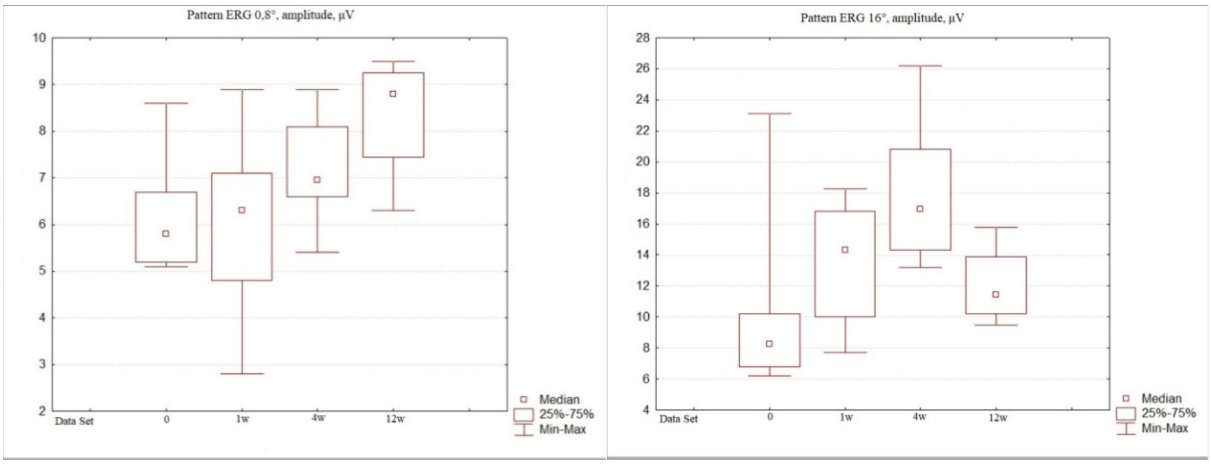

(a) **(b)**

Fig. 2. Box plot for medians of the transient PERGs amplitudes (μV) for stimuli 0.8° peak P50 **(a)** and 16° peak N95 **(b)** before (bottom, Set 0) and after one week (1w), one month (4w), and three months (12w) course of the FS.

The amplitude of rod ERG b-wave, on average in the group, showed a significant increase after the one-week ($p < 0.01$) and a one-month course of FS ($p < 0.001$). A reduction in the rod ERG b-wave peak latency was noted in the same time frame ($p < 0.01$ and $p < 0.05$ for weeks 1 and 4, respectively). After the 12 weeks-course of the FS, the amplitude and peak latency of the rod ERG b-wave retained their original values recorded before photostimulation. The dark-adapted ERG b-wave amplitude in the responses elicited to a standard stimulus (the maximal or mixed, rod-cone ERG) showed an increase after the 1 week ($p < 0.05$) and 12 weeks-courses ($p < 0.01$) of FS (Table 3, Fig. 3).

Table 3. Dark-adapted full-field ERGs (ISCEV Standard).

ERG scotopic 0.01, b-wave peak latency, ms									
Data Set	**Mean**	**Student's t-test**	**SD**	**Min**	**Max**	**Q25**	**Median**	**Q75**	**Mann-Whitney U-test**
0	66.66667		3.929207	61.10000	71.40000	64.00000	66.65000	70.20000	
1w	58.35000	***p* = 0.004182**	5.650398	54.00000	65.90000	54.00000	55.50000	65.20000	**0.041126**
4w	61.16667	***p* = 0.043839**	4.363790	56.40000	66.90000	56.40000	61.05000	65.20000	****0.064935***
12w	68.27500	*p* = 0.577748	2.280899	65.80000	70.50000	66.35000	68.40000	70.20000	0.609524
ERG scotopic 0.01, b-wave amplitude, μV									
Data Set	**Mean**	**Student's t-test**	**SD**	**Min**	**Max**	**Q25**	**Median**	**Q75**	**Mann-Whitney U-test**
0	171.6400		9.65935	156.4000	180.8000	169.7000	172.4000	178.9000	
1w	192.9600	***p* = 0.005672**	11.80267	182.6000	209.5000	183.2000	189.9000	208.9000	**0.007937**
4w	199.2667	***p* = 0.000528**	10.77806	190.8000	215.7000	191.0000	194.0500	210.0000	**0.004329**
12w	184.3000	*p* = 0.092885	9.54219	179.0000	198.6000	179.3000	179.8000	189.3000	0.11111
ERG scotopic 3.0, b-wave peak latency, ms									
Data Set	**Mean**	**Student's t-test**	**SD**	**Min**	**Max**	**Q25**	**Median**	**Q75**	**Mann-Whitney U-test**
0	40.78333		2.164640	38.20000	43.40000	39.30000	40.20000	43.20000	
1w	42.10000	*p* = 0.065433	4.353389	36.82000	45.60000	37.90000	41.15000	44.60000	0.240260
4w	39.40000	*p* = 0.423910	2.133542	37.00000	43.40000	38.70000	39.00000	39.30000	0.200186
12w	41.92500	***p* = 0.014034**	2.112463	40.00000	44.10000	40.40000	40.85000	43.55000	**0.009524**
ERG scotopic 3.0, b-wave amplitude, μV									
Data Set	**Mean**	**Student's t-test**	**SD**	**Min**	**Max**	**Q25**	**Median**	**Q75**	**Mann-Whitney U-test**
0	185.2200		9.61286	175.9000	199.7000	178.1000	183.0000	189.4000	
1w	199.0600	***p* = 0.034539**	10.75839	183.2000	209.2000	195.1000	199.1000	208.7000	****0.095238***
4w	189.6400	*p* = 0.467021	7.68622	181.7000	201.5000	184.1000	189.9000	191.0000	0.309524
12w	212.1667	***p* = 0.001459**	8.78085	204.8000	222.3000	206.8000	207.4000	221.2000	**0.035714**

** The tendency to decrease in the peak latency; * The tendency to increase in the amplitude;

Bold red – statistically significant ($p < 0.05$).

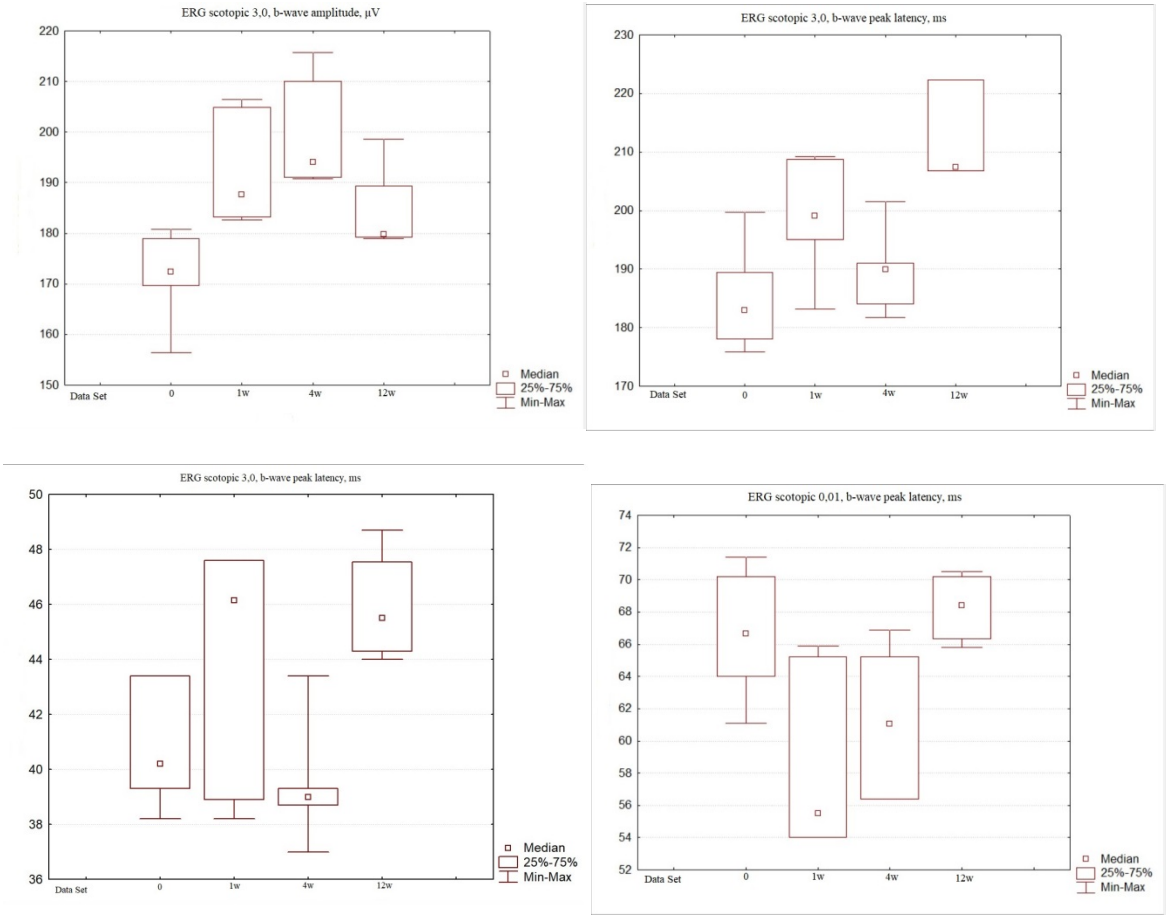

Fig. 3. Box plot for medians of the b-wave's amplitude (1, μV) and peak latency (2, ms) in the rod ERG 0.01 **(a)** and maximal scotopic ERG 3.0 **(b)** before (bottom, Set 0) and after one week (1w), one month (4w), and three months (12w) course of the FS.

The b-wave amplitude in the light-adapted ERG increased significantly - nearly 20% compared to the original values ($p < 0.01$) after the 4 and 12 weeks of FS (Table 4, Fig. 4), and showed a slight decrease in the peak latency ($p < 0.05$). The amplitude of the standard 30-Hz flicker ERG showed a significant enhancement at all points of observation on days 7 ($p < 0.01$), 30, and 90 ($p < 0.001$).

Table 4. Light-adapted full-field ERGs (ISCEV Standard).

ERG photopic 3.0, b-wave peak latency, ms									
Data Set	**Mean**	**Student's t-test**	**SD**	**Min**	**Max**	**Q25**	**Median**	**Q75**	**Mann-Whitney U-test**
0	30.33333		1.344123	28.40000	31.70000	29.10000	30.70000	31.40000	
1w	29.83333	$p = 0.331739$	0.450185	29.40000	30.50000	29.40000	29.75000	30.20000	0,484848
4w	29.23333	$\mathbf{p = 0.041560}$	0.463321	28.50000	29.90000	29.10000	29.25000	29.40000	0,240260
12w	29.12500	$\mathbf{p = 0.044848}$	0.903235	28.20000	29.90000	28.35000	29.20000	29.70000	0,171429
ERG photopic 3.0, b-wave amplitude, μV									
Data Set	**Mean**	**Student's t-test**	**SD**	**Min**	**Max**	**Q25**	**Median**	**Q75**	**Mann-Whitney U-test**
0	100.4800		8.55231	89.3000	111.3000	94.8000	103.5000	103.5000	

Table 4. *Cont.*

1w	108.4750	$p = 0.195736$	5.13055	105.0000	116.1000	105.5000	106.3500	111.4500	***0.085101***
4w	120.9333	**$p = 0.001765$**	10.16851	103.2000	133.0000	118.1000	121.7500	127.8000	**0.030303**
12w	119.9000	**$p = 0.004824$**	10.71391	110.9000	129.5000	112.5000	123.5000	129.3000	***0.071429***

***** The tendency to the increase in the amplitude; Bold red – statistically significant ($p < 0.05$).

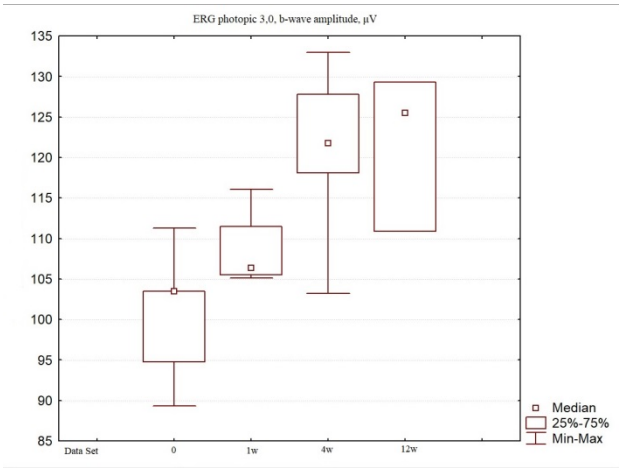

Fig. 4. Box plot for medians of the b-wave's amplitude (µV) in the light-adapted cone ERG before (bottom, Set 0) and after one week (1w), one month (4w), and three months (12w) course of the FS.

The photopic flicker ERGs recorded after a 4-week FS course manifested increased amplitude at all frequencies from 8.3 to 24 Hz (Table 5, Fig. 5).

Table 5. Photopic flicker ERGs on different frequencies of stimuli.

Flicker ERG 8.3 Hz, amplitude, µV									
Data Set	**Mean**	**Student's t-test**	**SD**	**Min**	**Max**	**Q25**	**Median**	**Q75**	**Mann-Whitney U-test**
0	109.1500		7.47819	101.9000	115.8000	102.7000	109.4500	115.6000	
1w	150.4750	**$p = 0.000001$**	2.09821	148.7000	153.5000	149.1500	149.8500	151.8000	**0.028571**
4w	170.1750	**$p = 0.000001$**	7.15419	161.1000	178.6000	165.8000	170.5000	174.5500	**0.020165**
12w	108.3333	$p = 0.853791$	3.06649	104.9000	110.8000	104.9000	109.3000	110.8000	0.999999
Flicker ERG 10 Hz, amplitude, µV									
Data Set	**Mean**	**Student's t-test**	**SD**	**Min**	**Max**	**Q25**	**Median**	**Q75**	**Mann-Whitney U-test**
0	98.9500		7.75392	92.3000	107.3000	92.3500	98.1000	105.5500	
1w	92.3333	$p = 0.241175$	5.84494	87.7000	98.9000	87.7000	90.4000	98.9000	0.228571
4w	139.2600	**$p = 0.000003$**	7.84015	128.0000	148.0000	137.4000	137.6000	145.3000	**0.015873**
12w	149.3667	**$p = 0.000001$**	4.65439	144.6000	153.9000	144.6000	149.6000	153.9000	***0.057143***
Flicker ERG 12 Hz, amplitude, µV									

Table 5. *Cont.*

Data Set	Mean	Student's t-test	SD	Min	Max	Q25	Median	Q75	Mann-Whitney U-test
0	96.9500		4.50888	92.9000	101.7000	93.1000	96.6000	100.8000	
1w	104.5500	$p = 0.223806$	9.21502	94.5000	115.1000	97.1000	104.3000	112.0000	0.342857
4w	129.5750	$\mathbf{p = 0.000177}$	9.96841	120.8000	138.7000	120.9500	129.4000	138.2000	**0.028571**
12w	125.3333	$\mathbf{p = 0.000967}$	8.68351	119.4000	135.3000	119.4000	121.3000	135.3000	***0.056333***
Flicker ERG 24 Hz, amplitude, Mv									
Data Set	**Mean**	**Student's t-test**	**SD**	**Min**	**Max**	**Q25**	**Median**	**Q75**	**Mann-Whitney U-test**
0	82.07500		7.98138	72.8000	92.2000	76.7000	81.6500	87.4500	
1w	80.76000	$p = 0.814334$	9.70763	64.7000	90.7000	80.7000	83.1000	84.6000	0.904762
4w	95.22500	$\mathbf{p = 0.041872}$	7.07030	86.3000	101.0000	89.5500	96.8000	100.9000	***0.054571***
12w	74.73333	$p = 0.261948$	6.40807	69.3000	81.8000	69.3000	73.1000	81.8000	0.400000

*The tendency to increase in the amplitude; Bold red – statistically significant ($p < 0.05$).

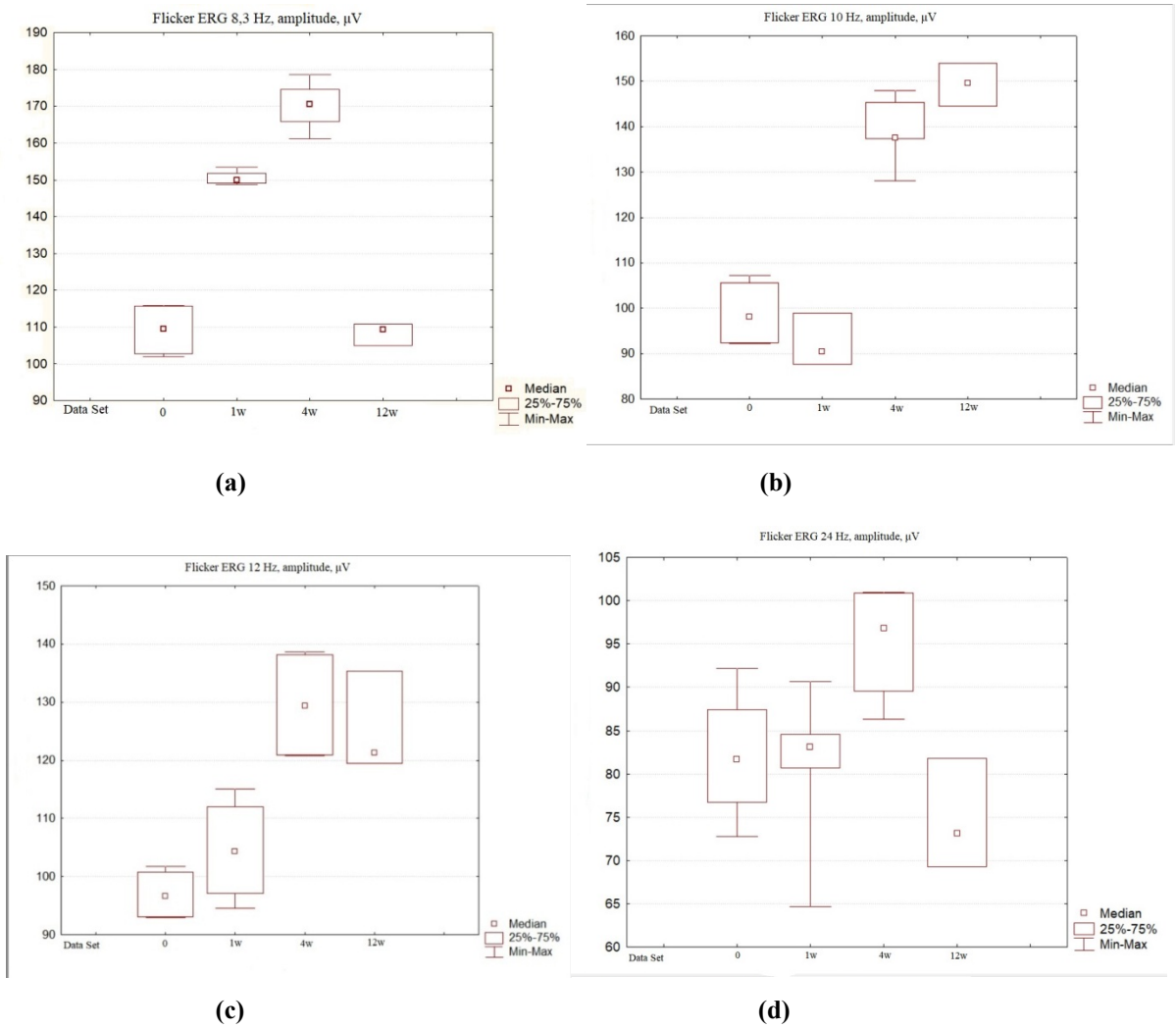

Fig. 5. Box plot for medians of the flicker ERG amplitude (µV) for the frequencies (a) 8.3 Hz, (b) 10 Hz, (c) 12 Hz, and (d) 24 Hz before (bottom, Set 0) and after one week (1 w), one month (4 w), and three months (12 w) course of the FS.

However, these alterations were statistically significant only for low-frequency flicker FERG (8.3, 10, and 12 Hz) but not for the ERG response to 24-Hz flickers. The most significant increase in amplitudes was noted for low-frequency flicker ERGs at 8.3 and 10 Hz ($p < 0.001$). The amplitude of the responses at 8.3 Hz was enhanced as early as one week into the FS course. The flicker ERGs at 10 and 12 Hz remained enhanced even after 90 days of the experiment.

4. Discussion

4.1. Optical Coherence Tomography

Rabbits are often used in studying retinal diseases and testing new therapeutic interventions. The physiology and morphology of the rabbit retina were well explored. It is known that rabbits have a 'visual streak', a zone where the density of photoreceptors is the highest – approximately 3 mm ventral to the optic nerve head [42–44,49]. The OCT allows quick and non-invasive determination of the retina architectonics by qualitative and quantitative analysis [50]. The advent of spectral OCT (SD-OCT) increased scanning speed and significantly improved image quality. In humans, when using 3D modeling in layer-by-layer verification of the retinal layers, the layer of retinal ganglion cells (GCS) and the inner plexiform layer (IPL) are also well scrutable along with their subsequent quantitative analysis. A tracking system allows significantly reducing visual noise [51,52], which improves the visualization of individual layers of the retina, including the layers of the outer and inner retina. The anatomical dimensions of the rabbit eye are closest to the human, which allows using the SD-OCT device without any additional attachments. The study does not require anesthesia of laboratory animals and allows analyzing the dynamics of retinal changes in vivo [53]. The presented research did not reveal any significant anatomical alterations in the retina even after a 3-month FS course. Thus, it can be assumed that even multi-day exposure to fractal optical signals is safe for the retinal structure and may be used in clinical studies without harm or overdose risk.

4.2. Electroretinography

No deterioration of retinal activity was observed compared with the base data after the FS sessions. The FS significantly increased the amplitudes and shortened the peak latencies of the scotopic and photopic ERGs' b-waves. The photostimulation with fractal signals increased flicker ERGs amplitudes at all frequencies. The results demonstrated the most considerable amplitude enhancement for the low-frequency ERG responses (8.3, 10, and 12 Hz). Since photoreceptor activity contribution dominates in the low-frequency flicker ERG [48], these data indicate the impact of photostimulation on the cone photoreceptors' activity. For the 8.3-Hz flicker ERG, the FS effect appeared after one week of FS and decreased for the 3-month FS course (compared to 1 month). The same dynamics were found also for the rod b-wave amplitude and peak time. Thus, the data indicate that in further studies of pathology on animal models and clinical research, a 4-week FS course is advisable. However, given that a significant increase in the 8.3-Hz and 30-Hz flicker ERG amplitudes was found already after 1 week of FS, fractal therapy lasting 1-2 weeks should be considered an alternative to the 30-day course in clinical trials.

The functional activity of retinal ganglion cells (RGCs) was evaluated by analyzing changes in the transient and steady-state PERG in this study. In healthy rabbits, the PERG amplitude is maximal for large-size stimuli [54]. In this study, the maximal PERG amplitude in healthy eyes of rabbits was also recorded for the 16° patterns and lower amplitudes - for stimuli with angular sizes of 0.8° and 0.3°. The PERG responses on the large-size stimuli may reflect the activity of large-field RGCs. ON and OFF alpha-RGCs described in rabbit retinas have large somas and wide dendritic branching in the inner plexiform layer [55–57]. The density of alpha cells has the maximal value (about 55/mm^2) in the visual streak [56]. However, the rabbit retina contains various types of RGCs that differ in morphology and physiology [58–60]. The slight FS impact for PERG amplitudes was noted in the responses to all pattern sizes after 1 month of FS and thus, theoretically to different RGCs types in the rabbit retina. However, the statistically significant effect was found only for stimulus 16°. The discovered effects of FS need to be tested in models of retinal pathology, where they may show other effects on the activity of the retinal cells.

4.3. Scientific Data Substantiating the Prospects of Using Stimulating Therapy with Fractal Visual Signals

Extensive evidence is currently available for nonlinear structures in natural objects and a healthy human body [8, 61–66], including the central nervous system [67–69]. Fractals are irregular geometric figures with features of self-similarity and scale invariance. The structure of a fractal object remains unchanged with the magnification in the image [61, 70–78]. A fractal dimension D characterizes fractal patterns by quantifying their complexity as a ratio of the change in detail to the change in scale. This term was first applied to describe complex geometric forms [61]. D values describe natural fractals in the wide range from 1.3 to 1.9.

However, the most common natural geometric fractals have D values of 1.3 to 1.5 [65], representing medium complexity, for example, for such natural patterns as branching trees, clouds, river beds, sea coastlines, mountain relief, and others.

Humans are both subjects and objects of the dynamic chaos of nature. Hence, the human spatial and temporal structure of incoming sensory information can be a key driver on which brain health depends [26]. The fractal visual surroundings largely determine the visual processing, perception, and developing behavioral patterns [66,70,79]. The essential fact is that the human visual system evolved to provide visual processing of the mid-range fractals dominated by nature [80]. Studies show that natural and artificial geometric fractals share a general principle of aesthetic appeal to the observer, which depends on the visual complexity of fractals. Most people prefer fractal images of medium complexity [65,66,81,82]. Aks and Sprott [81] observed a preferred fractal dimension of 1.3, noting that it is consistent with dominant fractal patterns in nature. The natural and man-generated geometric fractals (including art and architecture) with a mid-range D may affect the observer's physiological condition [65,83–85]. Individual differences in the visual perception of fractal objects could also be associated with genetic factors [86].

The aesthetic perception of fractals is different for exact and statistical fractals [65]. Hagerhall *et al.* [77], carrying out continuous recordings of the electroencephalogram (EEG), found that the EEG oscillations power in the alpha-band alters when a statistical fractal is transformed into its exact variant. Human visual processing improves when perceiving fractals with middle D values [74,87,88]. In quantitative EEG, amplification of the beta rhythm confirms that the viewer's attention is attracted by fractals D with a mean of 1.3 [78]. Moreover, the fractals with $D = 1.3$ induced the maximal EEG response increase in both alpha and beta ranges [77, 78, 80].

The fractal environment can suppress the physiological response to stress caused by external factors and other circumstances, and the reduction of this response is rather weakly dependent on the origin of the fractal and its structure [80,85]. Like geometric fractals are self-similar patterns that maintain the same form in different space scales [61], the fractal processes are self-similar in time scale. That can be seen in a graphical representation of their fluctuations at various time resolutions [89,90]. Complex fluctuations of physiological rhythms of a healthy body possess fractal properties [8–11,62].

The loss of fractal complexity of different anatomical structures and functional activity is associated with pathology and aging [8, 14–18]. This is also true for the retina and visual system, for example, for dynamics of neural discharge in the cat's visual system [67,91], complexity in the branching of retina vessels [92], and neural processes in the lateral geniculate nucleus [93]. Aberrant rhythmic activity of the RGCs (periodic rhythm instead of fractal dynamics) develops in massive degeneration of photoreceptors [94–97].

We suggest that an objectively existing relationship between the functioning of the CNS and the spatial-temporal structure of the visual and other sensory stimuli affect people for their whole life [26]. Thus, in stimulation therapy, optical signals with fractal structures have the potential to assist in restoring the visual system and brain function via activation of the neuroplasticity [25–27]. It seems logical to use fractal cues to synchronize the rhythms of physiological fluctuations with external rhythms in order to preserve, maintain, and restore their healthy complex dynamics. The impact of natural fractal patterns does not alleviate a person's condition in all clinical situations. In several cases, including diseases that cause maladaptive changes in the retinal structure, there may be a need to use an artificially created fractal environment. Dynamic visual fractals, such as fractal flickering, can help impact the visual system and serve as a basis for new diagnostics strategies and treatment of brain and retinal diseases [25–27,98].

Considering the literature data discussed above, signals with a mid-value fractal dimension from 1.3 to 1.5 may be the most promising for fractal-stimulating phototherapy. It is noteworthy that the most pleasant music has a fractal dimension close to 1.4 [99]. The present research used the fractal dimension of the optical signal brightness fluctuation, equal to 1.4. The research revealed a positive effect of FS on retinal activity, which is most significant with a 2- to 4-week course of FS. A significant secondary lead lies in the fact that a long-term FS (up to 3 months) has no adverse effects on the function and structure of the retina.

4.4. Remarks on Possible Mechanisms of Effects of Fractal Phototherapy

It is known that even a small help to the patient in the form of partial regeneration of the retina and neural connections, provided, for example, by neuroprotective therapy or implants, can improve visual functions and the well-being of a person. A small from the physician's point of view statistical effect can be highly significant for the patient. Maintaining and even partially improving visual functions is critical for improving patients' quality of life and social rehabilitation. We believe that the therapy using signals with fractal dynamics activates adaptive neuroplasticity and increases the efficiency of retinal neuroprotection and visual rehabilitation in degenerative diseases of the visual system and brain. The therapeutic effects of visual restoration using FS can be associated with synaptic and dendritic plasticity activation. Responses to FS may include strengthening and forming new synaptic connections according to the Hebbian theory [100,101], neuronal sprouting, and the increased complexity of dendritic branching in the inner retina and the lateral geniculate body. Hebb considered enhanced synaptic efficiency after repeated

stimulation of the postsynaptic cell by the presynaptic neuron as an explanation of synaptic plasticity and the neuronal adaptation during brain learning: “Cells that fire together wire together” [102].

The remodeling of neural connections is adaptive neuroplasticity that depends on visual experience. The FS can affect neurotrophic factors and enhances the expression of genes that control protein synthesis and neuronal signaling, as shown for electrostimulation. For instance, transcorneal electrostimulation leads to enhanced neurotrophic factors, inhibition of proinflammatory cytokines, and increased chorioretinal circulation [103]. It is assumed that further studies of retinal pathology in animal models reveal objective signs of adaptive retinal plasticity induced by fractal phototherapy. This preliminary experiment aimed to determine the effect of the prolonged course of fractal photostimulation on the retina function. Elucidating mechanisms behind the effects of FS on retinal structure and function must be the topic of further research. We assume that FS could become an effective technology of nondrug neuroprotective therapy, a possible alternative method to limit the structural and functional alterations in degenerative diseases of the retina and brain.

The increase in retinal activity found in FS for healthy retinas is still insufficient to clarify the therapeutic possibilities of the new method. However, the data obtained indicate the prospects for subsequent experimental and clinical studies aimed at studying the role of fractal phototherapy in the restoration of visual functions using the low-intensity FS. Considering the dynamics of all ERG indicators, the effect was most pronounced for the 1-week - 1-month course of FS, which needs to be used in further studies.

4.5. Limitations and Strengths of the Study

We investigated the effects of FS with presumably optimal parameters for their introduction into the clinic that were physiologically substantiated by literature data as safe and potentially most effective. The experimental study evaluated the safety of long-term stimulation courses with low-intensity fractal stimuli to recommend the method to the clinic. It offered a theoretically optimal range of course duration to avoid overdose and determine the period within which the doctor can safely maneuver the number of FS sessions for different patients. We studied the FS effects only in healthy animals. Therefore, despite the observed positive trend of the ERG’s parameters, we cannot judge the therapeutic impacts of the FS on the retina. The subsequent research in animal models of retinal pathology needs to be performed to state the retinal neurons whose activity is susceptible to fractal simulation and estimate the mechanisms of effects and recommended regimen of fractal visual therapy. The impact of FS in pathology needs to be considered based on the response of a healthy retina. Moreover, the effects also must be different for various retinal diseases, and the study must present separate tasks. Such research is necessary to study the therapeutic effects of fractal phototherapy and to substantiate its indications and recommendations for choosing individual exposure parameters. This pilot study solves a particular problem., and ~~However,~~ the result helps to design future clinical multimodal studies. In clinical research, it is necessary for each pathology and, perhaps, each patient to provide a personalized approach for selecting specific and optimal FS courses.

5. Conclusions

This study describes the effect of FS on the rabbit’s retina functional activity for the first time. Long-term stimulation with low-intensity optical signals of fractal dynamics with the D equal to 1.4 did not impair retinal function. The observed FS effects included a temporary decrease in peak latency and increased scotopic and photopic ERG amplitude. These changes can reflect the adaptive plasticity of the retina which needs to be confirmed in the animal models of retinal pathology and clinical trials. The research results indicate the advisability of the FS courses duration of 1 to 4 weeks in subsequent studies.

Author Contributions: Conceptualization, M.Z. and N.N.; methodology, M.Z. and I.T.; software, D.F.; validation, M.Z., D.F., and I.T.; formal analysis, D.F., V.K., and T.O.; investigation, D.F., V.K., I.T., and T.O.; data curating, N.N. and I.T.; writing – original draft preparation, M.Z. and D.F.; writing – review & editing, M.Z.; supervision, M.Z. and N.N.; project administration, V.N. All authors have read and agreed to the published version of the manuscript.

Funding: This research did not receive external funding.

Conflicts of Interest: The authors declare no conflict of interest.

References

1. Serruya, M.D.; Kahana, M.J. Techniques and devices to restore cognition. *Behav Brain Res* **2008**, *192*, 149. https://doi.org/10.1016/j.bbr.2008.04.007
2. Krawinkel, L.A.; Engel, A.K.; Hummel, F.C. Modulating pathological oscillations by rhythmic non-invasive brain stimulation – a therapeutic concept? *Front Syst Neurosci* **2015**, *9*, 33. https://doi.org/10.3389/fnsys.2015.00033

3. Sabel, B.A.; Flammer, J.; Merabet, L.B. Residual vision activation and the brain-eye-vascular triad: dysregulation, plasticity and restoration in low vision and blindness – a review. *Restor Neurol Neurosci* **2018**, *36*, 767–791. https://doi.org/10.3233/RNN-180880
4. Espinosa, J.S.; Stryker, M.P. Development and plasticity of the primary visual cortex. *Neuron* **2012**, *75*, 230–249. https://doi.org/10.1016/j.neuron.2012.06.009
5. Barlow, J.S. Rhythmic activity induced by photic stimulation in relation to intrinsical activity of the brain in man. *Electroencephalogr Clin Neurophysiol* **1960**, *12*, 317–326. https://doi.org/10.1016/0013-4694(60)90005-5
6. Huang, T. L.; Charyton, C. A comprehensive review of the psychological effects of brainwave entrainment. *Altern Ther Health Med* **2008**, *14*(5), 38–50.
7. Goldberger, A.L. Fractal variability versus pathologic periodicity: complexity loss and stereotypy in disease. *Perspect Biol Med* **1997**, *40*(4), 543–561. https://doi.org/10.1353/pbm.1997.0063
8. Goldberger, A.L.; Amaral, L.A.N.; Hausdorff, J.M.; Ivanov, P.C.; Peng, C.-K.; Stanley, H.E. Fractal dynamics in physiology: Alterations with disease and aging. *Proc Nat Acad Sci USA* **2002**, *99*, 2466–2472. https://doi.org/10.1073/pnas.012579499
9. Peng, C.K.; Mietus, J.; Hausdorff, J.M.; Havlin, S.; Stanley, H.E.; Goldberger, A.L. Long-range anticorrelations and non-Gaussian behavior of the heart-beat. *Physical Review Letters* **1993**, *70*, 1343–1346. https://doi.org/10.1103/PhysRevLett.70.1343
10. Peng, C.K.; Mietus, J.E.; Liu, Y.; Lee, C.; Hausdorff, J.M.; Stanley H.E.; *et al.* Quantifying fractal dynamics of human respiration: age and gender effects. *Ann Biomed Eng* **2002**, *30*, 683–692. https://doi.org/10.1114/1.1481053.
11. Yamamoto, Y.; Hughson, R.L. On the fractal nature of heart rate variability in humans: effects of data length and beta-adrenergic blockade. *Am J Physiol* **1994**, *266*(1Pt 2), R40–R49. https://doi.org/10.1152/ajpregu.1994.266.1.R40
12. Lipsitz, L.A.; Goldberger, A.L. Loss of "complexity" and aging. *JAMA* **1992**, *267*(13), 1806–1809.
13. Hausdorff, J.M.; Purdon, P.L.; Peng, C.K.; Ladin, Z.; Wei, J.W.; Goldberger, A.L. Fractal dynamics of human gait: stability of long-range correlations in stride interval fluctuation. *J. Appl. Physiol*. **1996**, *80*, 1448–1457. https://doi.org/10.1152/jappl.1996.80.5.1448
14. Hausdorff, J.M.; Mitchell, S.L.; Firtion, R.; Peng, C.-K.; Cudkowicz, M.E.; Wei, J.Y.; Goldberger, A.L. Altered fractal dynamics of gait: Reduced stride-interval correlations with aging and Huntington's disease. *J Applied Physiol* **1997**, *82*(1), 262–269. https://doi.org/10.1152/jappl.1997.82.1.262
15. Dauwels, J.; Srinivasan, K.; Reddy, M.R.; Nusha, T.; Vialatte, F.-B.; Latchoumane, C.; *et al.* Slowing and loss of complexity in Alzheimer's EEG: Two sides of the same coin? *Int. J. Alzheim Dis* 2011, Art 539621. https://doi.org/10.4061/2011/539621
16. Takahashi, A.C.; Porta, A.; Melo, R.C.; Quitério, R.J.; da Silva, E.; Borghi-Silva, A.; *et al.* Aging reduces complexity of heart rate variability assessed by conditional entropy and symbolic analysis. *Intern. Emerg. Med.* **2012**, *7*, 229–235. https://doi.org/10.1007/s11739-011-0512-z
17. Sleimen-Malkoun, R.; Temprado, J.J.; Hong, S.L. Aging induced loss of complexity and dedifferentiation: consequences for coordination dynamics within and between brain, muscular and behavioral levels. *Front Aging Neurosci* 2014, 27, 140. https://doi.org/10.3389/fnagi.2014.00140
18. Chen, Y.; Wang, W.; Zhao, X.; Sha, M.; Liu, Y.; Zhang, X.; *et al.* Age-Related Decline in the Variation of Dynamic Functional Connectivity: A Resting State Analysis. *Front Aging Neurosci* **2017**, *9*, 203. https://doi.org/10.3389/fnagi.2017.00203
19. Namazi, H.; Kulish, V.; Akrami, A. The analysis of the influence of fractal structure of stimuli on fractal dynamics in fixational eye movements and EEG signal. *Scientific Res*. **2016**, *6*, 26639. https://doi.org/10.1038/srep26639
20. Sejdić, E.; Fu, Y.; Pak, A.; Fairley, J.A.; Chau, T. The effects of rhythmic sensory cues on the temporal dynamics of human gait. *PLoS One* **2012**, *7*(8), e43104. https://doi.org/10.1371/journal.pone.0043104
21. Hunt, N.; McGrath, D.; Stergiou, N. The influence of auditory-motor coupling on fractal dynamics in human gait. *Sci. Rep*. **2014**, *4*, 5879. https://doi.org/10.1038/srep05879
22. Rhea, C.K.; Kiefer, A.W.; Wittstein, M.W.; Leonard, K.B.; McPherson, R.P.; Wright, W.G.; Haran, F.J. Fractal Gait Patterns Are Retained after Entrainment to a Fractal Stimulus. *PLoS One* **2014**, *9*(9), e106755. https://doi.org/10.1371/journal.pone.0106755
23. Hove, M.J.; Suzuki, K.; Uchitomi, H.; Orimo, S.; Miyake, Y. Interactive Rhythmic Auditory Stimulation Reinstates Natural 1/f Timing in Gait of Parkinson's Patients. *PLoS One* **2012**, *7*(3), e32600. https://doi.org/10.1371/journal.pone.0032600
24. Gilbert, C.D.; Li, W. Adult visual cortical plasticity. *Neuron* **2012**, *75*(2), 250–264. https://doi.org/10.1016/j.neuron.2012.06.030
25. Zueva, M.V. Dynamic fractal flickering as a tool in research of non-linear dynamics of the evoked activity of a visual system and the possible basis for new diagnostics and treatment of neurodegenerative diseases of the retina and brain. *World Appl Sci J* **2013**, *27*(4), 462–468. https://doi.org/10.5829/idosi.wasj.2013.27.04.13657
26. Zueva, M.V. Fractality of sensations and the brain health: the theory linking neurodegenerative disorder with distortion of spatial and temporal scale-invariance and fractal complexity of the visible world. *Front Aging Neurosci* **2015**, *7*, 135. https://doi.org/10.3389/fnagi.2015.00135

27. Zueva, M.V. Technologies of nonlinear stimulation: role in the treatment of diseases of the brain and the potential applications in healthy individuals. *Human Physiology* **2018**, *44*(3), 289–299. https://doi.org/10.1134/S0362119718030180
28. Francardo, V.; Schmitz, Y.; Sulzer, D.; Cenci M.A. Neuroprotection and neurorestoration as experimental therapeutics for Parkinson's disease. *Exp Neurol* **2017**, *298*, 137–147. https://doi.org/10.1016/j.expneurol.2017.10.001
29. Gidday, J.M. Adaptive plasticity in the retina: Protection against acute injury and neurodegenerative disease by conditioning stimuli. *Cond Med* **2018**, *1*(2), 85–97.
30. Zueva, M.V.; Karankevich, A.I. Stimulator with complex-structured optical signals and method of its use. Eurasian Patent N 035247 B1. 2020, Moscow: Eurasian Patent Organization (EAPO) Office.
31. ARVO Statement for the Use of Animals in Ophthalmic and Visual Research. Available online: http://www.arvo.org/about_arvo/policies/statement_for_the_use_of_animals_in_ophthalmic_and_visual_research/, Accessed 30 Oct 2016.
32. Principles on Good Laboratory Practice. OECD series on principles of Good Laboratory Practice and Compliance Monitoring. No 1. Available online: https://www.oecd.org/chemicalsafety/testing/oecdseriesonprinciplesofgoodlaboratorypracticeglpandcompliancemonitoring.htm (Accessed 27 November 2021).
33. Srinivasan, K.; Tikoo, K.; Jena, G.B. Good Laboratory Practice (GLP) Requirements for Preclinical Animal Studies. In *Essentials of Laboratory Animal Science: Principles and Practices*; Nagarajan, P., Gudde, R., Srinivasan R. (Eds); Springer: Singapore, 2021.
34. Rosolen, S. G.; Kolomiets, B.; Varela, O.; Picaud, S. Retinal electrophysiology for toxicology studies: applications and limits of ERG in animals and ex vivo recordings. *Exp Toxicol Pathol* **2008**, *60*(1), 17–32. https://doi.org/10.1016/j.etp.2007.11.012.
35. Charng, J.; He, Z.; Vingrys, A.J.; Fish, R.L.; Gurrell, R.; Bui, B.V.; Nguyen, C.T. Retinal electrophysiology is a viable preclinical biomarker for drug penetrance into the central nervous system. *J Ophthalmol* **2016**; *2016*, 5801826. https://doi.org/10.1155/2016/5801826
36. Michelson, N.J.; Kozai, T.D.Y. Isoflurane and ketamine differentially influence spontaneous and evoked laminar electrophysiology in mouse V1. *J Neurophysiol* **2018**, *120*, 2232–2245. https://doi.org/10.1152/jn.00299.2018
37. Linsenmeier, R.A.; Beckmann, L.; Dmitriev, A.V. Intravenous ketamine for long term anesthesia in rats. *Heliyon* **2020**, *6*(12), E05686. https://doi.org/10.1016/j.heliyon.2020.e05686
38. WS2812B Datasheet and Specifications (2016). Intelligent control LED integrated light source. WORLDSEMI CO.,LIMITED, Jan, 2016, V1.0. Available online: https://voltiq.ru/datasheets/WS2812B_datasheet_EN.pdf (13 January 2022).
39. Williams, J. Frequency-specific effects of flicker on recognition memory. *Neuroscience* **2001**, *104*, 283. https://doi.org/10.1016/s0306-4522(00)00579-0
40. Williams, J.; Ramaswamy, D.; Oulhaj, A. 10 Hz flicker improves recognition memory in older people. *BMC Neurosci*. **2006**, *7*(5), 21. https://doi.org/10.1186/1471-2202-7-21
41. Zueva, M.V.; Kovalevskaya, M.A.; Donkareva, O.V.; Karankevich, A.I.; Tsapenko, I.V.; Taranov, A.A.; Antonyan, V.B. Fractal Phototherapy in Neuroprotection of Glaucoma. *Ophthalmology in Russia* **2019**, *16*(3), 317–328. (In Russ.). https://doi.org/10.18008/1816-5095-2019-3-317-328
42. Marc, R.E. Neurochemical stratification in the inner plexiform layer of the vertebrate retina. *Vision Res* **1986**, *26*, 223–238. https://doi.org/10.1016/0042-6989(86)90017-9
43. Famiglietti, E.V.; Sharpe, S.J. Regional topography of rod and immunocytochemically characterized “blue" and “green" cone photoreceptors in rabbit retina. *Vis Neurosci* **1995**, *12*(6), 1151–1175. https://doi.org/10.1017/s0952523800006799
44. Rockhill, R.L.; Daly, F.J.; MacNeil, M.A.; Brown, S.P.; Masland, R.H. The Diversity of Ganglion Cells in a Mammalian Retina. *J Neurosci* **2002**, *22*(9), 3831-3843. https://doi.org/10.1523/jneurosci.22-09-03831.2002
45. McCulloch, D.L.; Marmor, M.F.; Brigell, M.G.; Hamilton, R.; Holder, G.E.; Rzekov, R.; Bach, M. ISCEV Standard for full-field clinical electroretinography (2015 update). *Doc Ophthalmol* **2015**, *130*(1), 1–12. https://doi.org/10.1007/s10633-014-9473-7
46. Gjörloff, K.; Andréasson, S.; Ehinger, B. Standardized full-field electroretinography in rabbits. *Doc Ophthalmol* **2004**, *109*(2), 163–168. https://doi.org/10.1007/s10633-004-3924-5
47. Bach, M.; Brigell, M.G.; Hawlina, M.; Holder, G.E.; Johnson, M.A.; McCulloch, D.L.; *et al.* ISCEV standard for clinical pattern electroretinography (PERG). *Doc Ophthalmol* **2013**, *126*, 1–7. https://doi.org/10.1007/s10633-012-9353-y
48. Zueva, M.V.; Neroev, V.V.; Tsapenko, I.V.; Sarygina, O.I.; Grinchenko, M.I.; Zaitseva, S.I. Topographic diagnosis of retinal dysfunction in case of rhegmatogenous retinal detachment by the rhythmic ERG method of a wide range of frequencies. *Russian Ophthalmological Journal (Rossiyskiy oftal’mologicheskiy zhurnal*.) **2009**, *1*(2), 18–23 (In Russ.).
49. Vaney, D.I.; Young, H.M.; Gynther, I.C. The rod circuit in the rabbit retina. *Vis Neurosci* **1991**, *7*, 141–154. https://doi.org/10.1017/s0952523800011019

50. Wojtkowski, M.; Bajraszewski, T.; Gorczynska, I.; Targowski, P.; Kowalczyk A.; Wasilewski, W.; Radzewicz, C. Ophthalmic imaging by spectral optical coherence tomography. *Am J Ophthalmol* **2004**, *138*, 412–419. https://doi.org/10.1016/j.ajo.2004.04.049
51. Sakamoto, A.; Hangai, M.; Yoshimura, N. Spectral-domain optical coherence tomography with multiple B-scan averaging for enhanced imaging of retinal diseases. *Ophthalmology* **2008**, *115*, 1071–1078. https://doi.org/10.1016/j.ophtha.2007.09.001
52. Hangai, M.; Yamamoto, M.; Sakamoto, A.; Yoshimura, N. Ultrahigh-resolution versus speckle noise-reduction in spectral-domain optical coherence tomography. *Opt Express* **2009**, *17*, 4221–4235. https://doi.org/10.1364/OE.17.004221
53. Muraoka, Y.; Ikeda, H.O.; Nakano, N.; Hangai, M.; Toda, Y. Real-Time Imaging of Rabbit Retina with Retinal Degeneration by Using Spectral-Domain Optical Coherence Tomography. *PloS One* 2012, *7*(4), e36135. https://doi.org/10.1371/journal.pone.0036135
54. Feghali, J.G.; Jin, J.C.; Odom, J.V. Effect of short-term intraocular pressure elevation on the rabbit electroretinogram. *Invest Ophthalmol Vis Sci* **1991**, *32*(8), 2184–2189.
55. Peichl, L. Alpha ganglion cells in mammalian retinae: common properties, species differences, and some comments on other ganglion cells. *Vis Neurosci* **1991**, *7*(1–2), 155–169. https://doi.org/10.1017/S0952523800011020
56. Famiglietti, E.V. Class I and class II ganglion cells of rabbit retina: A structural basis for X and Y (brisk) cells. *J Comp Neurol* **2004**, *478*, 323–346. https://doi.org/10.1002/cne.20268
57. Zhang, J.; Li, W.; Hoshi, H.; Mills, S.L.; Massey, S.C. Stratification of alpha ganglion cells and ON/OFF directionally selective ganglion cells in the rabbit retina. *Vis Neurosci* **2005**, *22*(4), 535–549. https://doi.org/10.1017/S0952523805224148
58. Amthor, F.R.; Takahashi, E.S.; Oyster, C.W. Morphologies of rabbit retinal ganglion cells with concentric receptive fields. *J Comp Neurol* **1989**, *280*, 72–96. https://doi.org/10.1002/cne.902800107
59. Amthor, F.R.; Takahashi, E.S.; Oyster, C.W. Morphologies of rabbit retinal ganglion cells with complex receptive fields. *J Comp Neurol* **1989**, *280*, 97–121. https://doi.org/10.1002/cne.902800108
60. Masland, R.H.; Martin, P.R. The unsolved mystery of vision. *Curr Biol* **2007**, *17*(15), R578–R579. https://doi.org/10.1016/j.cub.2007.05.040
61. Mandelbrot, B. The fractal geometry of nature. *Macmillan*, 1983.
62. Goldberger, A.L.; Rigney, D.R.; West, B.J. Chaos and fractals in human physiology. *Sci Amer* **1990**, *262*(2), 42–49. https://doi.org/10.1038/scientificamerican0290-42
63. Ivanov, P.C.; Amaral, L.A.N.; Goldberger, A.L.; Stanley, H.E. Stochastic feedback and the regulation of biological rhythms. *Europhys Lett* **1998**, *43*, 363–368. https://doi.org/10.1209/epl/i1998-00366-3
64. Hausdorff, J.M.; Peng, C.K.; Ladin, Z.; Wei, J.Y.; Goldberger, A.L. Is walking a random walk? Evidence for long-range correlations in stride interval of human gait. *J Appl Physiol* **1995**, *78*, 349. https://doi.org/10.1152/jappl.1995.78.1.349
65. Taylor, R.P.; Spehar, B.; Wise, J.A.; Clifford, C.W; Newell, B.R.; Hagerhall, C.M.; *et al.* Perceptual and physiological responses to the visual complexity of fractal patterns. *Nonlinear Dynamics Psychol Life Sci* **2005**, *9*(1), 89–114. https://doi.org/10.1007/978-3-322-83487-4_4
66. Taylor, R.P.; Spehar, B.; von Donkelaar, P.; Hagerhall, C.M. Perceptual and physiological responses to Jackson Pollock's fractals. *Front Hum Neurosci* **2011**, *5*, 1–13. https://doi.org/10.3389/fnhum.2011.00060
67. Teich, M.C.; Heneghan, C.; Lowen, S.B.; Ozaki, T.; Kaplan, E. Fractal character of the neural spike train in the visual system of the cat. *J Opt Soc Am A* **1997**, *14*(3), 529–546. https://doi.org/10.1364/josaa.14.000529
68. Lehnertz, K. Non-linear time series analysis of intracranial EEG recordings in patient with epilepsy — an overview. *Int J Psychophysiol* **1999**, *34*, 45–52. https://doi.org/10.1016/s0167-8760(99)00043-4
69. Rabinovich, M.I.; Abarbanel, H.D. The role of chaos in neural systems. *Neuroscience* **1998**, *87*(1), 5–14. https://doi.org/10.1016/s0306-4522(98)00091-8.
70. Field, D.J. Relationships between the statistics of natural images and the response properties of cortical cells. *J Opt Soc Am* **1987**, *4*, 2379–2394.
71. Feder, J. *Fractals* (*Physics of Solids and Liquids*); Berlin: Springer, 1988, 284p.
72. Bassingthwaighte, J.B.; Liebovitch, L.S.; West, B.J. *Fractal Physiology*; Oxford: New York, 1994.
73. Crownover, R.M. *Introduction to Fractals and Chaos*; Jones and Bartlett Publishers: Boston - London, 1995, 306 p.
74. Field, D.J.; Brady, N. Visual sensitivity, blur and the sources of variability in the amplitude spectra of natural scenes. *Vis Res* **1997**, *37*, 3367–3383. https://doi.org/10.1016/s0042-6989(97)00181-8
75. Ruderman, D.L. Origins of scaling in natural images. *Vis Res* **1997**, *37*, 3385–3398. https://doi.org/10.1016/S0042-6989(97)00008-4
76. West, G.B.; Brown, J.H.; Enquist, B.J. The fourth dimension of life: fractal geometry and allometric scaling of organisms. *Science* **1999**, *284*, 1677–1769. https://doi.org/10.1126/science.284.5420.1677

77. Hagerhall, C.M.; Laike, T.; Küller, M.; Marcheschi, E.; Boydston, C.; Taylor, R.P. Human physiological benefits of viewing nature: EEG responses to exact and statistical fractal patterns. *Nonlinear Dynamics Psychol Life Sci* **2015**, *19*(1), 1–12.
78. Hagerhall, C.M.; Laike, T.; Taylor, R.P.; Küller, M.; Küller, R.; Martin, T.P. Investigation of EEG response to viewing fractal patterns. *Percept* **2008**, *37*, 1488–1494. https://doi.org/10.1068/p5918
79. Spehar, B.; Clifford, C.; Newell, B.; Taylor, R.P. Universal aesthetic of fractals. *Copmuters & Graphics* **2003**, *27*(5), 813–820. https://doi.org/10.1016/S0097-8493(03)00154-7
80. Taylor, R.P. The potential of biophilic fractal designs to promote health and performance: A review of experiments and applications. *Sustainability* **2021**, *13*, 823. https://doi.org/10.3390/su13020823
81. Aks, D.; Sprott, J. Quantifying aesthetic preference for chaotic patterns. *Empir. Stud. Arts* **1996**, *14*(1), 1–16. https://doi.org/10.2190/6V31-7M9R-T9L5-CDG9
82. Taylor, R.P.; Sprott, J.C. Biophilic fractals and the visual journey of organic screen-savers. *Nonlinear Dynamics Psychol. Life Sci* **2008**, *12*, 117–129. https://doi.org/10.1002/9781118257685.ch10
83. Wise, J. A., and Rosenberg E. The Effects of Interior Treatments on Performance Stress in Three Types of Mental Tasks. Technical Report, Space Human Factors Office, NASA-ARC, Sunnyvale, CA, 1986.
84. Taylor, R.P. Reduction of physiological stress using fractal art and architecture. *Leonardo* **2006**, *39*(3), 245–251. https://doi.org/10.1162/leon.2006.39.3.245
85. Salingaros, N.A. Fractal art and architecture reduce physiological stress. *Journal of Biourbanism* **2012**, *2*, 11–28.
86. Pyankova, S.D.; Chertkova, Y.D.; Scobeyeva, V.A.; Chertkova, E.R. Influence of Genetic Factors on Perception of Self-similar Objects. *Psychol Subculture Phenomenol Contemp Tendencies Dev* **2019**. https://doi.org/10.15405/epsbs.2019.07.69
87. Knill, D.C.; Field, D.; Kersten, D. Human discrimination of fractal images. *J. Opt Soc Am* **1990**, *7*(6), 1113–1123. https://doi.org/10.1364/josaa.7.001113
88. Geake, J.; Landini, G. Individual differences in the perception of fractal curves. *Fractals* **1997**, *5*(1), 129–143. https://doi.org/10.1142/S0218348X97000139
89. Belair, J.; Glass, L.; van der Heiden, U.; Milton, J. *Dynamical Disease: Mathematical Analysis of Human Illness*; American Institute of Physics Press: New York 1995.
90. Beuter, A.; Glass, L.; Mackey, M.; Titcombe, M.S. *Nonlinear Dynamics in Physiology and Medicine*; Springer-Verlag: New York, 2003.
91. Lowen, S.B.; Ozaki, T.; Kaplan, E.; Saleh, B.E.A.; Teich, M.C. Fractal features of dark, maintained, and driven neural discharges in the cat visual system. *Methods* **2001**, *24*, 377–394. https://doi.org/10.1006/meth.2001.1207
92. Cheung, N.; Donaghue, K.C.; Liew, G.; Rogers, S.L.; Wang, J.J.; Lim, S.W.; *et al.* Quantitative assessment of early diabetic retinopathy using fractal analysis. *Diabetes Care* **2009**, *32*(1), 106–110. https://doi.org/10.2337/dc08-1233
93. Ly, T.; Gupta, N.; Weinreb, R.N.; Kaufman, P.L.; Yücel, Y.H. Dendrite plasticity in the lateral geniculate nucleus in primate glaucoma. *Vis Res* **2011**, *51*(2), 243–250. https://doi.org/10.1016/j.visres.2010.08.003
94. Strettoi, E.; Porciatti, V.; Falsini, B.; Pignatelli, V.; Rossi, C. Morphological and functional abnormalities in the inner retina of the rd/rd mouse. *J Neurosci* **2002**, *22*(13), 5492–5504. https://doi.org/10.1523/jneurosci.22-13-05492.2002
95. Menzler, J.; Channappa, L.; Zeck, G. Rhythmic ganglion cell activity in bleached and blind adult mouse retinas. *PLoS One* **2014**, *9*(8), e106047. https://doi.org/10.1371/journal.pone.0106047
96. Ivanova, E.; Yee, C.W.; Baldoni, R.; Sagdullaev, B.T. Aberrant activity in retinal degeneration impairs central visual processing and relies on Cx36- containing gap junctions. *Exp Eye Res* **2016**, *150*:81–89. https://doi.org/10.1016/j.exer.2015.05.013
97. Zeck G. Aberrant activity in degenerated retinas revealed by electrical imaging. *Front Cell Neurosci* **2016**, *10*, 25. https://doi.org/10.3389/fncel.2016.00025
98. Cheng, W.; Law, P. K.; Kwan, H.C.; Cheng, R.S. Stimulation therapies and the relevance of fractal dynamics to the treatment of diseases. *Open J Regenerative Medicine* **2014**, *3*(4), 73–94. https://doi.org/10.4236/ojrm.2014.34009
99. Hazard, C.; Kimport, C.; Johnson, D. Fractal Music. Research Project. 1998–1999, Available online: http://www.tursiops.cc/fm (Accessed August 2015), https://ru.scribd.com/document/309739163/Fractal-Music (Accessed January 2022).
100. Hebb, D.O. *The Organization of Behavior*; Wiley & Sons: New York, 1949, 335p. https://doi.org/10.1002/1097-4679(195007)6:3<307::AID-JCLP2270060338>3.0.CO;2-K
101. Morris, R.G. D.O. Hebb: The Organization of Behavior, Wiley: New York; 1949. *Brain Res Bull* **1999**, *50*(5–6),437. https://doi.org/10.1016/s0361-9230(99)00182-3.
102. Löwel, S.; Singer, W. Selection of intrinsic horizontal connections in the visual cortex by correlated neuronal activity. *Science* **1992**, *255*(5041), 209–212. https://doi.org/10.1126/science.1372754

103. Sehic, A.; Guo, Sh.; Cho, K.-S.; Corraya, R.M.; Chen D.F.; Utheim, T.P. Electrical stimulation as a means for improving vision. *Am J Pathol* **2016**, *186*, 2783e2797. https://doi.org/10.1016/j.ajpath.2016.07.017